ORIGINAL RESEARCH PAPER

Removal of Cobalt Ions from Contaminated Water Using Magnetite Based Nanocomposites: Effects of Various Parameters on the Removal Efficiency

Saeed Tizro, Hadi Baseri*

School of Chemistry, Damghan University, Damghan, Iran.

Received: 2016-12-13 Accepted: 2017-04-20 Published: 2017-07-10

ABSTRACT

Cobalt is one of the most hazardous heavy metals present in the environment. Magnetic based nanoadsorbents were used for removal of Co(II) ions in this work. The characteristics results of FT-IR, XRD, TGA, and FE-SEM show that applied coatings were modified magnetite nanoparticles efficiently. The results of TEM indicate that magnetic nanoadsorbents were produced on the nanoscale with average particle sizes of 60±10 nm. Batch experiments were carried out to determine the removal efficiency of the nanoadsorbents. pH, temperature, contact time, adsorbent dose, shaking rate and the initial concentration of analyte were the studied parameters. At optimized conditions of operation parameters, the maximum removal percentage of 92% was obtained by using magnetite-citric acid as an adsorbent. Equilibrium data for Co(II) ions adsorption onto magnetite-citric acid were fitted well by Langmuir isotherm model and the maximum adsorption capacity for Co(II)ions was obtained 43.292 mg/g at 313 K. Also, thermodynamic parameters reveal the spontaneity, feasibility and endothermic nature of the Co(II) ions adsorption process. In addition, the cobalt ions can be desorbed from magnetite-citric acid nanoadsorbent by using nitric acid solution with 95% desorption efficiency and the magnetite-citric acid nanoadsorbent exhibits good recyclability.

Keywords: *Adsorption, Cobalt ions, Contaminated Water, Magnetite*

How to cite this article

Tizro S, Baseri H. Removal of Cobalt Ions from Contaminated Water Using Magnetite Based Nanocomposites: Effects of Various Parameters on the Removal Efficiency. J. Water Environ. Nanotechnol., 2017; 2(3): 174-185. DOI: 10.22090/jwent.2017.03.005

INTRODUCTION

Cobalt is a very toxic heavy metal ion and it´s containing compounds are widely used in many industrial applications such as mining, electroplating, metallurgical, paints, pigments and electronic [1]. The permissible limits of cobalt in the livestock wastewater and irrigation water are 1.0 and 0.05 mg/L, respectively [2]. The presence of cobalt in the environment leads to several health troubles such as low blood pressure, vomiting, nausea, heart diseases, vision problems, sterility, thyroid damage, hair loss, bleeding, diarrhea, bone defects and may also cause mutations (genetic changes) in living cells [2,3]. So the fast and effective removal of Co(II) from the aqueous solution is necessary for the environmental protection. There are several different techniques for the removal of Co(II) ions, such as chemical precipitation, oxidation, ion-exchange, reverse osmosis, membrane electrolysis, coagulation and adsorption [5-9]. Among these available techniques, adsorption method has been used widely, because it is simple, adaptable, economical, and cost-effective. So many materials such as clay minerals, oxides, activated carbon, zeolites, ion exchange resin and cellulose have been used as adsorbents [10-14]. Low adsorption

*Corresponding Author Email: baseri@du.ac.ir

capacity and difficult separation are the problems that limit the application of these materials.

Recently, magnetite-based nanocomposite adsorbents have been fabricated and have shown good properties for drug delivery [15] energy storage [16,17] and water treatment[18]. Also, the use of magnetite-based nanoadsorbents in water treatment provides a suitable and comfortable approach for separating and removing the pollutants by applying an external magnetic field.

This present study pursues: (1) synthesis of different magnetite-based nanoadsorbents by using co-precipitation method; (2) characterization of these adsorbents by using Fourier transform infrared spectroscopy (FT-IR), X-ray diffractometer (XRD), Field emission scanning electron microscopy (FE-SEM),thermogravimetric (TGA) analysis and Transmission electron microscopy (TEM); (3) study the effects of main parameters that affect adsorption of Co(II) ions; (4) study isotherm, thermodynamic and kinetic parameters of adsorption process and (5) study reusability and stability of nanoadsorbents. The main object of this work is to develop cost efficient, biocompatible and easily available adsorbent for the environmental applications.

EXPERIMENTAL

Materials

Ferric chloride ($FeCl_3 \cdot 6H_2O$), ferrous sulfate ($FeSO_4 \cdot 7H_2O$), ammonia solution (with analytical grade, Merck Chemical Company) and double-distilled water were used for the preparation of magnetite nanoparticles. Natural zeolite clinoptilolite was prepared from the West Semnan, Iran and all of the coatings (citric acid ($C_6H_8O_7$), ascorbic acid ($C_6H_8O_6$), salicylic acid ($C_7H_6O_3$), starch $(C_6H_{10}O_5)_n$ and saccharose ($C_{12}H_{22}O_{11}$)) were purchased from the Sigma–Aldrich company.

Synthesis of magnetite-based nanoadsorbents

We used previously reported co-precipitation method [19] for the synthesis of bare magnetite nanoparticles. In order to synthesize Fe_3O_4 based nanoadsorbents (except magnetite-zeolite), 4.2 g of $FeSO_4.7H_2O$ and 6.1 g of $FeCl_3.6H_2O$ were dissolved in 100 mL of double-distilled water and heated at 100 °C for 1 h. After that 10 mL of ammonium hydroxide solution (25%) was added to the mixture. Then the temperature of the system decreased to the 80 °C and 0.5 g of the coating was dissolved in 50 mL of distilled water and was added to the mixture. The mixture was stirred at this temperature for about 1 hour. The dark brown precipitate was collected by centrifugation and washed with deionized water and acetone for 3 times and dried at 70°C for 5 h.

Magnetite-clinoptilolite nanoadsorbent was prepared by the co-precipitation method as follows: First of all, for activation of natural zeolite, 10 mL of H_2SO_4-HCl (%10) solution was added to the zeolite and the mixture was relaxed for 3 h. Then acid was evacuated and the sample was washed with deionized water 2 times and dried at 200°C for about 3 h. We added the activation zeolite to the Fe_3O_4 sample. Centrifugation, washing and drying processes of the obtained sample were done just like the last samples and the final product´s color was dark brown.

Characterization

The surface functional groups of samples were determined by Fourier transform infrared spectrum (Spectrum RXI).The crystal structures of the synthesize nanoadsorbents were determined by XRD analysis (D8-Advance, Bruker AXS, Cu K α1, λ=1.54 °A). The thermogravimetric analyses of the samples were performed with a thermal analysis system (STA 503). For these measurements, the weight losses of dried samples were monitored under N_2 from room temperature to 600 °C at a rate of 10°C/min. Surface study and size measurement of the nanostructures were done by Field emission scanning electron microscopy (Hitachi S4160) and transmission electron microscopy (Philips CM 30), respectively. Atomic adsorption spectroscopy (Chemtech analytical CTA-2000) was used for determination of Co(II) ions concentration in supernatant.

Batch adsorption experiments

In order to evaluate the adsorption ability of synthesized nanoadsorbents, batch experiments were carried out at room temperature. Hydrated $Co(NO_3)_2$ was used as the source of Co(II) ions and pH values were adjusted by using 0.1 M NaOH or 0.1 M HCl. In a typical removal experiment, 0.2 g of magnetite-citric acid nanoadsorbent was added into 100 mL of Co(II) ions solution (25 mg/L), sealed and shaken for 1 h(rpm was 500). Then as can be seen from Fig. 1, magnetite was easily separated by using an external magnetic field. Co(II) ions concentration in the supernatant solution was measured by using atomic absorption

spectroscopy. All of the experiments were carried out in triplicates and average values were used in the graphs. The adsorption capacity and removal percentage of Co(II) ions were calculated by using Eqs. (1) and (2), respectively [20,21].

$$q_e = \frac{(C_0 - C_e)}{W} x\, V \quad (1)$$

$$\text{Removal efficiency (\%)} = \frac{(C_0 - C_e)}{C_0} x\, 100 \quad (2)$$

Where q_e (mg/g) is the adsorption capacity at equilibrium, C_0 and C_e are the initial and equilibrium concentration of Co(II) ions (mg/L); V is the total volume of solution in (L) and W is the adsorbent mass(g).

RESULT AND DISCUSSION

Characterization of nanoadsorbents

The crystalline structures of differently synthesized nanoadsorbents were identified with XRD pattern (Fig. 2). Diffraction peaks with 2θ at 30.2°, 35.5°, 43.3°, 57.2°, and 62.8°that were observed for bare magnetite spectra, indicate a cubic spinel structure of this nanoparticle [22]. The same set of characteristic peaks were also observed for magnetite-citric acid, magnetite-salicylic acid and magnetite-starch samples that indicate the stability of the crystalline phase of magnetite nanoparticles during functionalization of the surface [23]. The magnetite-clinoptilolite pattern shows three crystalline peaks with 2θ at 35°, 58° and 62° related to the 311, 511 and 440 crystallographic planes of the face-centered cubic (FCC) iron oxide nanocrystals [24]. The average crystallite size of different nanoadsorbents was calculated by using the Scherrer's equation [25]:

$$D_c = \frac{0.9\,\lambda}{L.\ \mathrm{Cos}\theta_B} \quad (3)$$

Where D_c is the crystallite size (A°), λ is 1.54056

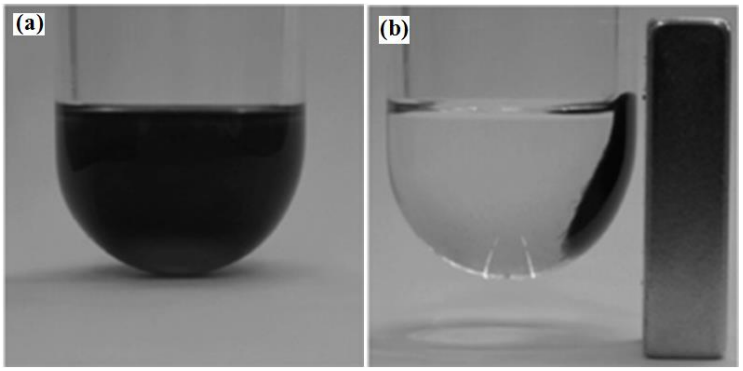

Fig. 1. Magnetic nanoadsorbent separation in Co(II) ions media (a) before using magnet, (b) after using magnet

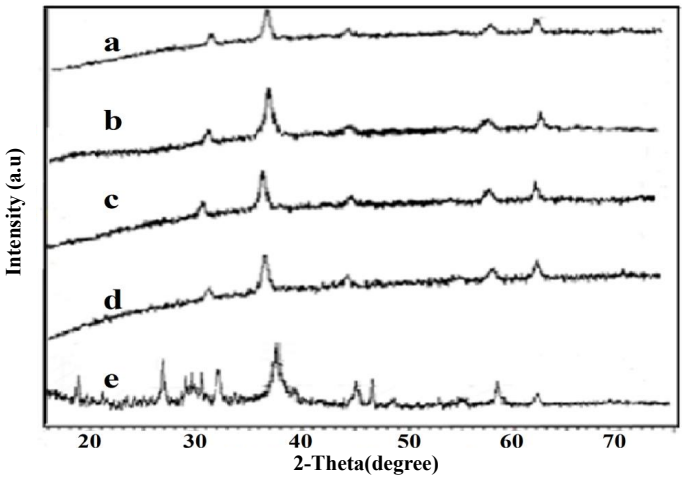

Fig. 2. XRD pattern of (a) bare magnetite, (b) magnetite-citric acid, (c) magnetite-salicylic acid, (d) magnetite-starch and (e) magnetite-clinoptilolite

A° , L is the full width at half-maximum (FWHM) and Θ_B is Bragg angle. Obtained results are summarized in Table 1.

The FT-IR spectra of bare magnetite nanoparticles, magnetite-citric acid, magnetite-salicylic acid, magnetite-starch, and magnetite-clinoptilolite are illustrated in Fig. 3. The low-intensity adsorption band at 570 cm^{-1}attributed to Fe-O stretching vibration of the magnetite nanoparticles was observed in all five samples [26,27]. The observed band at nearly 3500 cm^{-1} in bare magnetite spectra is due to –OH stretching vibrations. There is a large and intense band at nearly 3450 cm^{-1} in magnetite-citric acid sample spectra that could be devoted to the structural OH groups of molecular water or citric acid. The intense band at nearly 1600 cm^{-1} for the magnetite-citric acid, revealed the binding of a citric acid radical to the magnetite surface (Fig. 3b). In the spectrum of magnetite-salicylic acid (Fig. 3c), the two peaks that were observed at 2850 and 2920 cm^{-1} were corresponded to the asymmetric and symmetric CH_2 stretching vibrations, respectively [28]. In the magnetite-starch spectra (Fig. 3d), the peak that was observed at 1090 concerned with the C-O stretching vibration in the C-O-H group, while the

Table 1. Average crystallite size of different nanoadsorbents.

Nanoadsorbents	Average crystallite size (nm)
Bare magnetite	16
Magnetite-citric acid	19
Magnetite-salicylic acid	18
Magnetite-starch	19
Magnetite-clinoptilolite	20

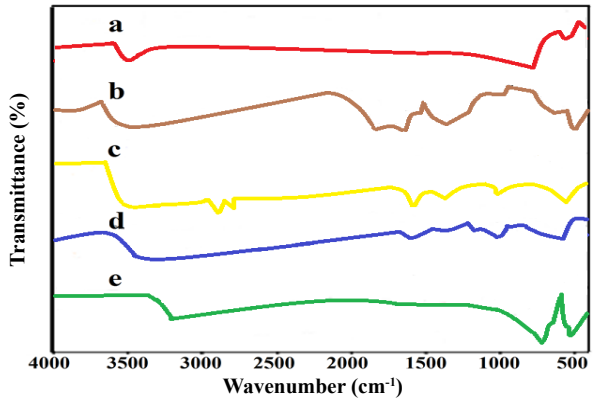

Fig. 3. FT-IR spectra of (a) bare magnetite, (b) magnetite-citric acid, (c) magnetite-salicylic acid, (d) magnetite-starch and (e) magnetite-clinoptilolite

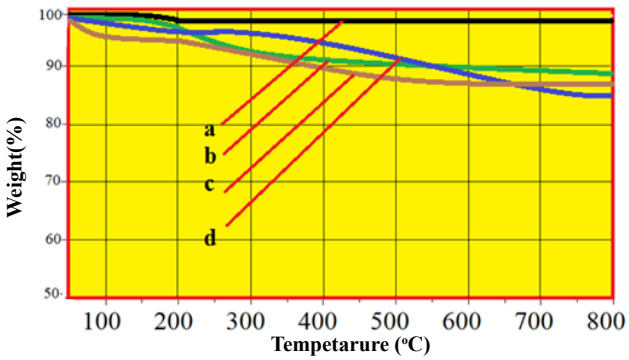

Fig. 4. TGA curve for(a) bare magnetite, (b) magnetite-citric acid, (c) magnetite-salicylic acid and (d) magnetite-starch

1160 cm^{-1} peak corresponded to the C-O stretching vibration in the C-O-C group. Unlike the bare magnetite sample, the greatly intensified peaks were observed for the magnetite-starch sample due to the H-bonded OH groups of amylose and amylopectin of starch [29]. In comparison with magnetite, FTIR spectrum of magnetite-clinoptilolite in the range of 440-580 cm^{-1} showed vibration bands that related to Fe-O functional groups (Fig. 3e).

TGA curves of bare magnetite, magnetite-citric acid, magnetite-salicylic acid and magnetite-starch were shown in Fig. 4. TGA curve of the bare magnetite nanoparticles shows a weight loss of about 2% below 200°Cwhich can be attributed to the loss of adsorbed water in the sample and no other weight loss was observed until 800 °C. TGA curve for Fe_3O_4-citric acid exhibits two steps of weight loss. The first weight loss can be attributed to the loss of residual water in the sample and the second is due to the loss of citric acid in the range of 200 to 600 °C. The total weight loss for this sample is about 12%. For the magnetite-salicylic acid sample, a weight loss of about 4% is observed between room temperature and 200 °C, which is attributed to the evaporation of adsorbed water. A secondary weight loss of about 10% in the temperature range of 200 to 600 °C is attributed to the decomposition of salicylic acid. For Fe_3O_4-starch sample, weight loss at temperatures below 250°C can be attributed to water desorption and a drastic weight loss of about 13% from 250 to 600 °C is due to the loss or decomposition of starch. The obtained TGA curves of these samples confirm the successful modifications of magnetite nanoparticles.

SEM images of the magnetite-ascorbic acid sample are shown in Figs. 5(a) and 5(b). MNPs are roughly spherical and tend to aggregate together because of their high surface energy and adhesion.

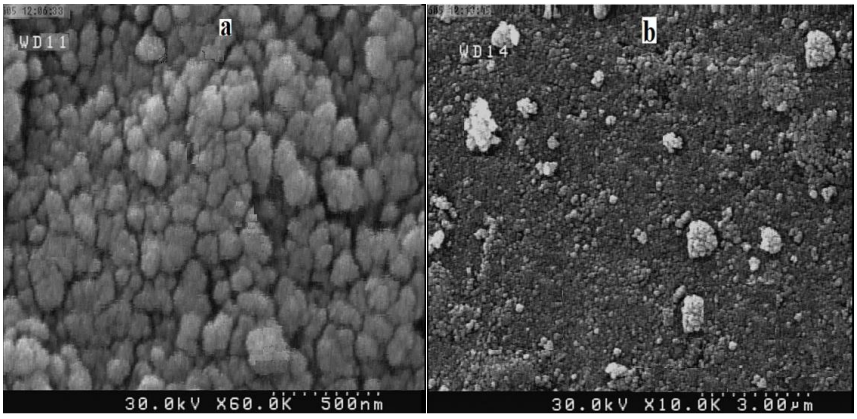

Fig. 5. SEM images of magnetite-ascorbic acid

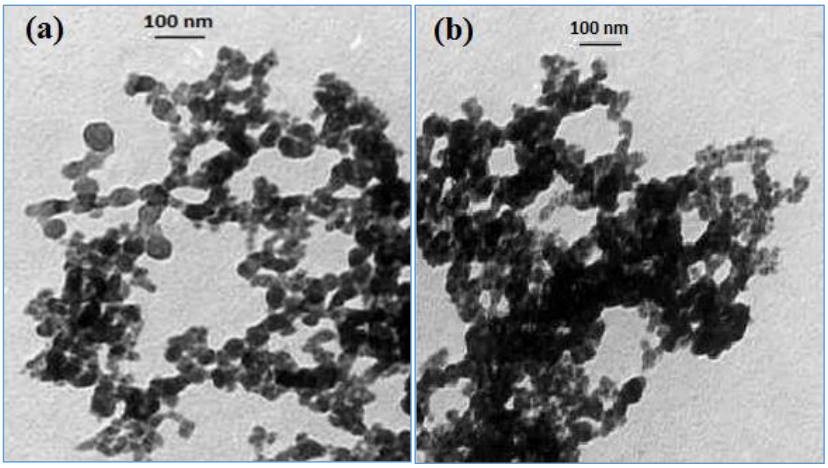

Fig. 6. TEM image of (a) bare magnetite nanoparticles, (b) ascorbic acid coated magnetic nanoparticles

TEM images of magnetite and magnetite-ascorbic acid are shown in Fig. 6a and 6b, respectively. Well-shaped spherical or ellipsoidal magnetic nanoparticles are observed in TEM images. Particle size distribution histogram is presented in Fig. 7 which is obtained by measuring 100 nanoparticles. An average size of 60±10 nm was obtained for magnetite-ascorbic acid nanoparticles. Crystallite size obtained from XRD pattern is smaller than the particle size obtained from TEM, revealing the polycrystalline structure of most observed nanoparticles. Also, the similar size of magnetite with magnetite-ascorbic acid indicates that the binding process did not result in agglomeration and the change in the size of the nanoparticles.

Adsorption study using nanoadsorbents

Some of the main parameters affecting the Co(II) ions adsorption by using synthesized nanoadsorbents were investigated and optimized here. These parameters are pH, temperature, contact time, adsorbent dose, shaking rate and initial concentration of the analyte.

Effect of pH

pH is a key factor affecting the adsorption of heavy metal ions. So, the dependence of pH on the removal of Co(II) ions was studied at a constant Co(II) ions concentration (25 mg./L) using 0.2g of nanoadsorbent. As shown in Fig. 8, cobalt adsorption increased with increase in pH range from 2 to 8 and slowly decreased or fixed with increasing pH in the range of 8 to 12. Therefore, pH 8 was chosen for further experiments. The removal decreasing trend at pH above 8 can correspond to nanoadsorbents probable destroying in an alkaline environment and certain precipitation of $Co(OH)_2$ from the solution. At pH higher than 8, the dominance of OH^- ions in the solution creates a competition between negatively charged nanoadsorbent surface and OH^-

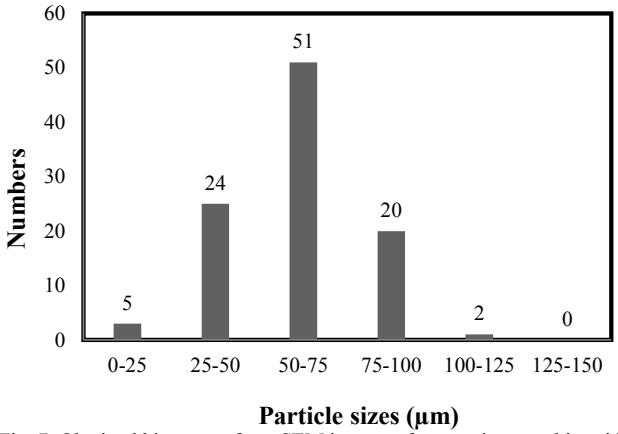

Fig. 7. Obtained histogram from SEM images of magnetite-ascorbic acid

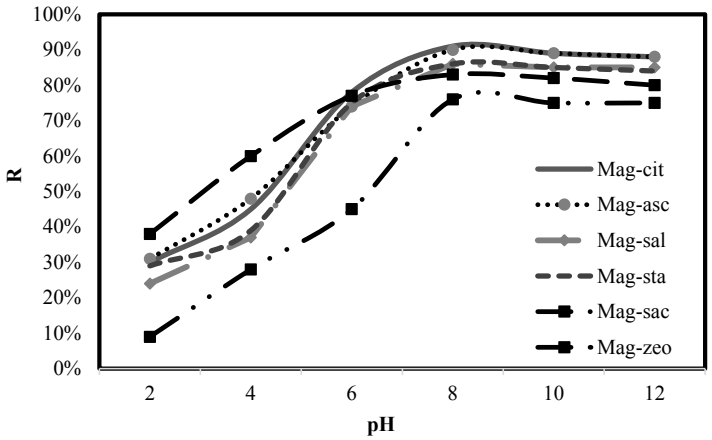

Fig. 8. Effect of pH on the removal of Co(II) (adsorbents dose: 0.2 g, Co(II) concentration: 25 mg/L)

ions which resulted in a decrease in the adsorption of Co(II) metal ions[31]. The suppressed adsorption of metal ions at lower pH implies that acid treatment is a possible and useful method to regenerate these nanoadsorbents [32,33].

Effect of temperature

The effects of temperature on the adsorption of Co(II) ions were explained in Fig. 9. It was observed that removal increased with increase in the temperature range from 293 to 313 K and further fixed or even slowly decreased at the higher temperatures. Probably the connivance decrease in the removal of Co(II) ions that observed at higher temperatures was due to the weakening of the adsorptive forces between the active sites on the nanoadsorbents surfaces and Co(II) ions[24].

Effect of contact time

Fig. 10 shows the time-dependent behavior of Co(II) ions removal from aqueous solution by using different synthesized adsorbents. As shown, the removal amount of Co(II) ions increased with increase in contact time and the equilibrium time was reached within 50 min. The initial adsorption rate was very fast which was due to the existence of a greater number of available sites on nanoadsorbents surfaces for Co(II) ions adsorption. According to the obtained results contact time of 50 min selected for further experiments.

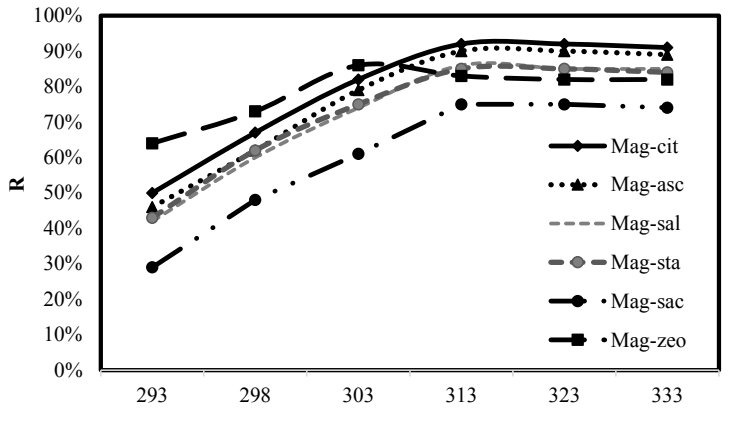

Fig. 9. Effect of temperature on the removal of Co(II) (adsorbents dose: 0.2 g, Co(II) concentration: 25 mg/L).

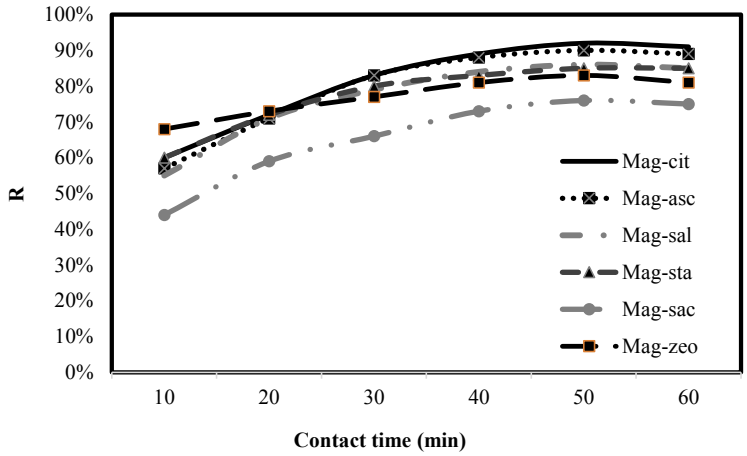

Fig. 10. Effect of contact time on the removal of Co(II) (adsorbents dose: 0.2 g, Co(II) concentration: 25 mg/L).

Effect of adsorbent dose

In order to study the adsorbent dose effect on the removal of Co(II) ions, the adsorption experiments were carried out with different concentrations of nanoadsorbents. 40, 80, 120, 160, 200 and 240 mg of each magnetite based nanoadsorbents were applied. As can be seen from Fig. 11, by increasing the dose of the nanoadsorbents, the number of adsorption sites available for adsorbent interaction is increased, thereby resulting in the increased percentage of Co(II) ions removal from the solution. In all cases, the optimal amount of adsorbent dose was 0.2 g and no significant increase was observed with further increases in adsorbent dose.

Effect of shaking rate

Since an optimum shaking rate is essentially needed to maximize the interactions between metal ions and adsorption sites of nanoadsorbents, the removal of Co(II) ions under various shaking rates was investigated and is shown in Fig. 12. It is found that Co(II) ions removal increased with increase in shaking rates from 100 to 500 rpm and with further increases in shaking rate from 500 to 750 rpm, the effect of shaking rate on the cobalt adsorption became comparatively negligible. This can be explained by the fact that, for a relatively lower shaking rate, the system is incompletely mixed; hence the poor dispersion of nanoparticles in solution resulted in only a small portion of surface area of adsorbent being exposed and reacted with the Co(II) ions. With further increasing the shaking rate from 500 to 750 rpm, the effect of shaking rate on the Co(II) adsorption became comparatively insignificant; since the system was well mixed under a comparatively higher shaking

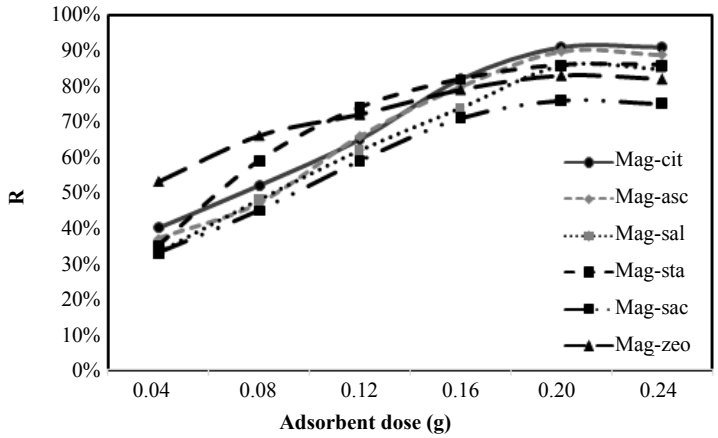

Fig. 11. Effect of adsorbent dosage on the removal of Co(II)

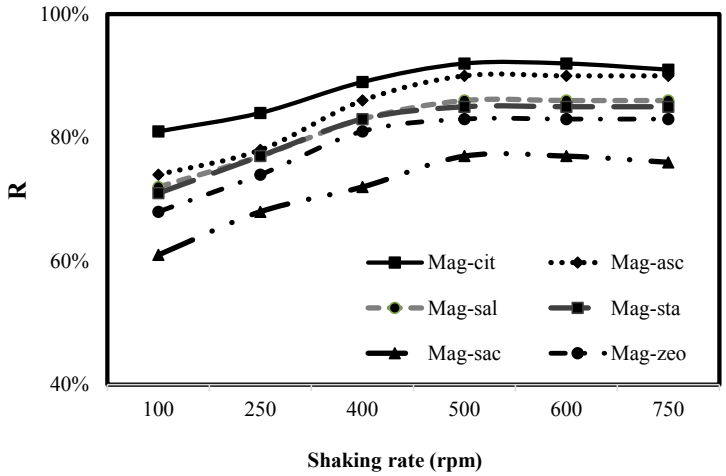

Fig. 12. Effect of shaking rate on the removal of Co(II) (pH: 8, Co(II) concentration: 25 mg/L).

rate, say 500 rpm[34]. As a consequence, a shaking rate of 500 rpm was selected as the optimum value and was used for further experiments.

Effect of initial concentration

The initial concentration of the analyte is also an important parameter for removal of heavy metals. As shown in Fig. 13, by increasing the initial concentration of Co(II) ions, removal amounts were decreased. Regarding maximum removal of Co(II) ions at 25 mg/L concentration of the analyte and a further significant decrease in removal amounts, 25 ppm was selected for further studies.

After obtaining optimum values of different parameters, we did the Co(II) ions adsorption by using bare magnetite nanoparticles. Removal efficiency was obtained 69% in this situation. From obtained results, it is completely clear that magnetite-citric acid is the most efficient adsorbent among the tested materials for the removal of Co(II) ions. So we did further studies just by using this nanoadsorbent.

Adsorption isotherms

Cobalt adsorption is significantly influenced by the initial concentration of Co(II) ions in aqueous solution. In this study, the initial concentration of Co(II) ions varied from 10 to 100 mg/L while the adsorbent dosage is 0.2 g/L, pH is 8 and contact time is 50 min. The experimental data were fitted to Langmuir [35] and Freundlich [36] isotherm model.

The Langmuir isotherm model was used to describe the chemisorptions and monolayer coverage of adsorbates onto nanoadsorbents and it is linear form can be expressed by the following equation:

$$\frac{C_e}{q_e} = \frac{1}{K_L q_m} + \frac{1}{q_m} C_e \quad (4)$$

Where q_e is the amount of Co(II) adsorbed at equilibrium in mg/g, C_e is the solute equilibrium concentration in mg/L, $q_{max,}$ and K_L is Langmuir constants indicating the saturated capacity of adsorbents and energy term, respectively.

The Freundlich isotherm model which indicates the exponential distribution of active sites and their energies and surface heterogeneity of the adsorbents are described by the following equation:

$$q_e = K_f C_n^{1/n} \quad (5)$$

Where K_f and $1/n$ are the Freundlich constants related to the adsorption capacity and the adsorption intensity, respectively.

Table 2 shows that the adsorption behavior of Co(II) ions onto the magnetite-citric acid nanoadsorbent is better described by Langmuir isotherm model because this model yields higher correlation coefficients. This indicates that monolayer coverage of magnetite-citric acid adsorbent is the main sorption mechanism.

The maximum adsorption capacity determined by the Langmuir model was 43.292 mg/g which was compared with other reports in Table 3.

Thermodynamic parameters

The effect of temperature on the adsorption isotherm was investigated under isothermal conditions in the temperature range of 303to 323

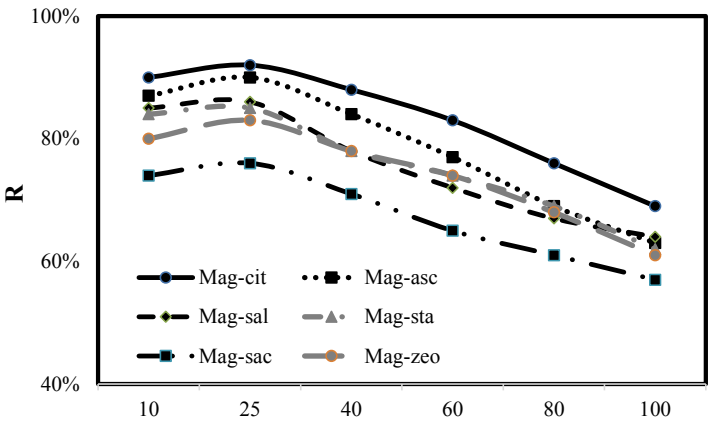

Fig. 13. Initial concentration effect on removal of Co(II).

K and optimal pH, contact time and adsorbent dose. Thermodynamic parameters such as change in free energy () (KJ/mol), enthalpy () (KJ/mol), and entropy () (J/mol.K) are calculated using the following thermodynamic functions [44,45]:

$$\Delta G^0 = -RT \ln K_d \quad (6)$$

$$\ln K_d = -\frac{\Delta H^0}{RT} + \frac{\Delta S^0}{R} \quad (7)$$

$$K_d = \frac{q_e}{C_e} \quad (8)$$

$$\Delta G^0 = \Delta H^0 - T\Delta S^0 \quad (9)$$

where R is the universal gas constant (8.314 J/mol.K), T is the absolute temperature in Kelvin, K_d is distribution coefficient, (mg/g) is the equilibrium concentration of Co(II) ions adsorbed onto magnetite-citric acid and (mg/L) is the remained concentration of Co(II) ions in the aqueous solution. The values of the different thermodynamic parameters are summarized in Table 4. value was obtained 47.684 kJ/mol and it means that adsorption process has endothermic nature [46]. The negative and positive values indicate the spontaneous nature of the adsorption process and affinity of the Co(II) ions adsorbent [47,48], respectively. The value of decreases with increase in temperature suggesting that higher temperature makes the adsorption process favourable but this stop at temperature upper than 323 K (Fig. 9).The positive entropy change for the process is caused by the increase in degree of freedom or randomness at the adsorbent-adsorbate interface during the adsorption of Co(II) ions at different temperatures [49].

Kinetic parameters

The adsorption kinetics of Co(II) ions onto magnetite-citric acid is investigated with the help of the pseudo-first order [50] and pseudo-second order [51] model.

The linear form of pseudo-first order kinetic model is expressed by the following equation:

$$\ln(q_e - q_t) = \ln q_t - k_1 t \quad (10)$$

Where q_e and q_t refer to the adsorption capacity of Co(II) ions (mg/g) at equilibrium and at any time, respectively and k_1 is the rate constant of pseudo-first order adsorption (1/min).

The pseudo-second-order kinetic rate equation

Table 2. Isotherm parameters for the adsorption of cobalt on magnetite-citric acid adsorbent

Temperature (K)	Langmuir model			Freundlich model		
	K_L(L/mg)	q_m(mg/g)	R^2	N	K_F (mg/kg)(L/mg)^(1/n)	R^2
293	0.08	27.84	0.995	1.32	1.90	0.983
303	0.11	34.32	0.998	1.60	4.02	0.985
313	0.13	43.29	0.999	1.68	5.38	0.971

Table 3. Comparison of adsorption capacity (mg/g) of different adsorbents for removal of Co(II) ions.

Adsorbent	Adsorption capacity (mg/g)	Reference
Kaolinite	0.92	[37]
Coir pith	12.82	[38]
Natural zeolites	14.38	[39]
EDTA-modified silica gel	20.00	[40]
Synthetic hydroxyapatite	20.19	[41]
Lemon peel adsorbent	22.00	[42]
Fe_3O_4/GO	22.70	[43]
Al-pillared bentonite clay	38.60	[1]
Present study	43.29	-

Table 4. Thermodynamic parameters for the adsorption of cobalt on magnetite-citric acid adsorbent

Temperature(K)	ΔG^0(kJ/mol)	ΔH^0(kJ/mol)	ΔS^0(J/mol.K)
303	-6.25	47.68	0.18
313	-6.74		
323	-7.16		

Table 5. Kinetic parameters for the adsorption of cobalt on magnetite-citric acid adsorbent.

Pseudo-first order				Pseudo-second order		
k_1 (min^{-1})	$q_{e.cal}$ (mg/g)	R^2	$q_{e,exp}$	k_2 (min^{-1})	$q_{e.cal}$ (mg/g)	R^2
0.06	8.34	0.995	13.72	0.01	13.41	0.998

is expressed as follows:

$$\frac{t}{q_t} = \frac{1}{k_2 q_e^2} + \frac{1}{q_e} t \qquad (11)$$

Where k_2 is the rate constant of pseudo-second order adsorption (g/mg.min).

As can be seen from Table 5, the adsorption of Co(II) ions onto magnetite-citric acid is more favorably described by a pseudo-second-order kinetic model because of its greater correlation coefficient (0.998) and closer values of calculated and experimental q_e. The higher values of R^2 of pseudo-second order and applicability of Langmuir isotherm indicated that the process to be chemisorptions in nature [45,52,53].

Stability and reusability of nanoadsorbents

To evaluate desorption of Co(II) ions loaded magnetite-citric acid, various concentration of 0.05, 0.1, 0.15 and 0.2 M HNO_3 was used as desorption media and quantitative desorption efficiencies were 72%, 92%, 94% and 95%, respectively. The maximum value of desorption efficiency was 95% by using 0.20 M concentrate of HNO_3. To evaluate the reusability of adsorption–desorption process, five times desorption were carried out. In this study, the initial concentration of Co(II) ions was 25 mg/L, the adsorbent dose was 0.2 g, the reaction temperature was 298 K, pH was 3 and shaking rate was 500 rpm. In each experiment, the used magnetite-citric acid nanoadsorbent was collected by using an external magnet. Obtained results that are summarized in Table 6 show a wonderful reusability for selected nanoadsorbent. It was observed that with an increase in cycle numbers, uptake capacity of Co(II) ions was slowly decreased. Following reaction was used in order to determine the efficient recovery of Co(II) ions:

$$R(\%) = \frac{C_{des}}{C_{ads}} \times 100 \qquad (12)$$

Table 6. Reusability of magnetite-citric acid for adsorption/ desorption of Co(II) ions during five cycles

Cycle numbers	Removal percentage
1	92
2	92
3	91
4	90
5	90

CONCLUSION

The main idea of this study was to provide a simple, cost-effective, reproducible and inexpensive method to remove Co(II)ions from aqueous solution. To this end, different magnetic nanocomposites were synthesized by the simple co-precipitation method. Some of these nanoadsorbents weren´t synthesized until now. After determining and characterizing of different synthesized nanoadsorbents structure, several parameters affecting the removal of Co(II) ions were evaluated and optimized. The results show that in all cases, the maximum removal efficiency of Co(II) ions was obtained by using magnetite-citric acid as an adsorbent. Also, the results show that pH, temperature, contact time, adsorbent dose and initial concentration factors have a high effect on the removal of Co(II) ion. It is found that the adsorption behavior of Co(II) ions is better described by the Langmuir isotherm model and the kinetics of Co(II) ions adsorption follows the pseudo-second order model. Moreover, the results indicate that the method has a suitable repeatability and nanoadsorbents have high stability. Results of this work suggest that the magnetite-based nanoadsorbents are wonderful adsorbents for the removal of heavy metal ions from synthetic and industrial wastewater by using the technology of magnetic separation.

CONFLICT OF INTEREST

The authors declare that there are no conflicts of interest regarding the publication of this manuscript.

REFERENCES

1. Sayadi MH, Rezaei MR. Impact of land use on the distribution of toxic metals in surface soils in Birjand city, Iran. Proceedings of the International Academy of Ecology and Environmental Sciences. 2014;4(1):18-29.

2. Sayadi MH, Rezaei MR, Rezaei A. Fraction distribution and bioavailability of sediment heavy metals in the environment surrounding MSW landfill: a case study. Environmental Monitoring and Assessment. 2014;187(1):4110.

3. Sayadi MH, Rezaei MR, Rezaei A. Sediment Toxicity and Ecological Risk of Trace Metals from Streams Surrounding a Municipal Solid Waste Landfill. Bulletin of Environmental Contamination and Toxicology. 2015;94(5):559-63.

4. Sayadi MH, Shabani M, Ahmadpour N. Pollution Index and Ecological Risk of Heavy Metals in the Surface Soils of Amir-Abad Area in Birjand City, Iran. Health Scope. 2015;4(1):ee21137.

5. Ghaleno OR, Sayadi M, Rezaei M, Kumar CP, Somashekar R, Nagaraja B. Potential ecological risk assessment of heavy metals in sediments of water reservoir case study: Chah Nimeh of Sistan. Proc Int Acad Ecol Environ Sci. 2015;5(4):89-96.

6. Mohan D, Pittman Jr CU. Arsenic removal from water/ wastewater using adsorbents—A critical review. Journal of Hazardous Materials. 2007;142(1–2):1-53.

7. Sayadi M, Torabi S. Geochemistry of soil and human health: A review. Pollution Research. 2009;28(2):257-62.

8. Smedley PL, Kinniburgh DG. A review of the source, behaviour and distribution of arsenic in natural waters. Applied Geochemistry. 2002;17(5):517-68.

9. Nordstrom DK. Worldwide Occurrences of Arsenic in Ground Water. Science. 2002;296(5576):2143-5.

10. Organization WH. Guidelines for drinking-water quality. Vol. 1, Recommendations. 3rd ed: World Health Organization; 2004.

11. Wang P, Sun G, Jia Y, Meharg AA, Zhu Y. A review on completing arsenic biogeochemical cycle: Microbial volatilization of arsines in environment. Journal of Environmental Sciences. 2014;26(2):371-81.

12. Nguyen TV, Vigneswaran S, Ngo HH, Pokhrel D, Viraraghavan T. Specific Treatment Technologies for Removing Arsenic from Water. Engineering in Life Sciences. 2006;6(1):86-90.

13. Bhargavi RJ, Maheshwari U, Gupta S. Synthesis and use of alumina nanoparticles as an adsorbent for the removal of Zn(II) and CBG dye from wastewater. International Journal of Industrial Chemistry. 2015;6(1):31-41.

14. Bissen M, Frimmel FH. Arsenic — a Review. Part II: Oxidation of Arsenic and its Removal in Water Treatment. Acta hydrochimica et hydrobiologica. 2003;31(2):97-107.

15. Akin I, Arslan G, Tor A, Ersoz M, Cengeloglu Y. Arsenic(V) removal from underground water by magnetic nanoparticles synthesized from waste red mud. Journal of Hazardous Materials. 2012;235–236:62-8.

16. Kanel SR, Manning B, Charlet L, Choi H. Removal of Arsenic(III) from Groundwater by Nanoscale Zero-Valent Iron. Environmental Science & Technology. 2005;39(5):1291-8.

17. Rahmani A, Ghaffari H, Samadi M. A comparative study on arsenic (III) removal from aqueous solution using nano and micro sized zero-valent iron. Iranian Journal of Environmental Health Science & Engineering. 2011;8(2):157-66.

18. Pena M, Meng X, Korfiatis GP, Jing C. Adsorption Mechanism of Arsenic on Nanocrystalline Titanium Dioxide. Environmental Science & Technology. 2006;40(4):1257-62.

19. Li Q, Easter NJ, Shang JK. As(III) Removal by Palladium-Modified Nitrogen-Doped Titanium Oxide Nanoparticle Photocatalyst. Environmental Science & Technology. 2009;43(5):1534-9.

20. Ghosh D, Luwang MN. Arsenic detection in water: YPO4:Eu3+ nanoparticles. Journal of Solid State Chemistry. 2015;232:83-90.

21. Martinson CA, Reddy KJ. Adsorption of arsenic(III) and arsenic(V) by cupric oxide nanoparticles. Journal of Colloid and Interface Science. 2009;336(2):406-11.

22. Shrivas K, Shankar R, Dewangan K. Gold nanoparticles as a localized surface plasmon resonance based chemical sensor for on-site colorimetric detection of arsenic in water samples. Sensors and Actuators B: Chemical. 2015;220:1376-83.

23. JANBAZ FM, KHOLGHI M, HORFAR A, HAGHSHENAS D. EXPERIMENTAL INVESTIGATION OF ARSENIC REMOVAL BY USING FE NANO PARTICLES IN BATCH EXPERIMENT. journal of Environmental Studies. 2014;39(4):149-56.

24. Koohpayehzadeh H, Torabian A, Nabi Bidhendi G, Habashi N. Nanoparticle Zere-valent Iron Affect on As (V) Removal from Drinking Water. Journal of Water and Wastewater(parallel title); Ab va Fazilab (in persian). 2012;23(3):60-7.

25. Olyaie E, Banejad H, Rahmani AR, Afkhami A, Khodaveisi J. Feasibility study of using Calcium Peroxide Nanoparticles in Arsenic Removal from Polluted Water in Agriculture and It's Effect on the Irrigation Quality Parameters Iranian Journal of Health and Environment. 2012;5(3):319-30.

26. Adlim M, Abu Bakar M, Liew KY, Ismail J. Synthesis of chitosan-stabilized platinum and palladium nanoparticles and their hydrogenation activity. Journal of Molecular Catalysis A: Chemical. 2004;212(1–2):141-9.

27. De Corte S, Hennebel T, Fitts JP, Sabbe T, Bliznuk V, Verschuere S, et al. Biosupported Bimetallic Pd–Au Nanocatalysts for Dechlorination of Environmental Contaminants. Environmental Science & Technology. 2011;45(19):8506-13.

28. Arsiya F, Sayadi MH, Sobhani S. Green synthesis of palladium nanoparticles using Chlorella vulgaris. Materials Letters. 2017;186:113-5.

29. Rahmani A, Ghaffari H, Samadi M. Removal of Arsenic (III) from Contaminated Waterby Synthetic Nano Size Zerovalent Iron. World Academy of Science, Engineering and Technology, International Journal of Environmental, Chemical, Ecological, Geological and Geophysical Engineering. 2010;4(2):96-9.

30. Goswami A, Raul PK, Purkait MK. Arsenic adsorption using copper (II) oxide nanoparticles. Chemical Engineering Research and Design. 2012;90(9):1387-96.

31. Sartape AS, Mandhare AM, Jadhav VV, Raut PD, Anuse MA, Kolekar SS. Removal of malachite green dye from aqueous solution with adsorption technique using Limonia acidissima (wood apple) shell as low cost adsorbent. Arabian Journal of Chemistry.

32. Sajadi F, Sayadi MH, Hajiani M. Study of optimizing the process of Cadmium adsorption by synthesized silver nanoparticles using Chlorella vulgaris. Journal of Birjand University of Medical Sciences. 2016;23(2):119-29.